Highly efficient, spectrally pure 340 nm ultraviolet emission from $Al_xGa_{1-x}N$ nanowire based light emitting diodes

2013 Nanotechnology 24 345201

(http://iopscience.iop.org/0957-4484/24/34/345201)

Nanotechnology **24** (2013) 345201 (6pp) doi:10.1088/0957-4484/24/34/345201

Highly efficient, spectrally pure 340 nm ultraviolet emission from $Al_xGa_{1-x}N$ nanowire based light emitting diodes

Q Wang, A T Connie, H P T Nguyen, M G Kibria, S Zhao, S Sharif, I Shih and Z Mi

Department of Electrical and Computer Engineering, McGill University, 3480 University Street, Montreal, Quebec, H3A 0E9, Canada

E-mail: zetian.mi@mcgill.ca

Received 28 May 2013, in final form 21 June 2013
Published 30 July 2013
Online at stacks.iop.org/Nano/24/345201

Abstract

High crystal quality, vertically aligned $Al_xGa_{1-x}N$ nanowire based double heterojunction light emitting diodes (LEDs) are grown on Si substrate by molecular beam epitaxy. Such $Al_xGa_{1-x}N$ nanowires exhibit unique core–shell structures, which can significantly suppress surface nonradiative recombination. We successfully demonstrate highly efficient $Al_xGa_{1-x}N$ nanowire array based LEDs operating at ∼340 nm. Such nanowire devices exhibit superior electrical and optical performance, including an internal quantum efficiency of ∼59% at room temperature, a relatively small series resistance, highly stable emission characteristics, and the absence of efficiency droop under pulsed biasing conditions.

(Some figures may appear in colour only in the online journal)

1. Introduction

Recently, optoelectronic devices in the ultraviolet (UV) spectral region have demonstrated an enormous amount of potential in applications for biosensors and medical devices. Among these emerging applications, highly efficient, spectrally pure UV emission at 340 nm is of critical importance. For example, it is ideally suited for the optical determination of the reduced nicotinamide adenine dinucleotide (NADH), a key constituent molecule found in all living cells, that has a strong absorbance at 340 nm and a fluorescence emission peak at ∼460 nm [1–3]. An ultra-compact 340 nm optoelectronic excitation source is desired to be integrated into a nanobiosensor for disease diagnosis via NADH fluorescence testing [4, 5]. In addition, a biocompatible implantable UV light source represents one of the key components of future medical devices to optically control neurons and/or to perform photolysis of photolabile caged compounds such as neurotransmitters, nucleotides, Ca^{2+} chelators, γ-aminobutyric acid (GABA) and fluorescent dyes [6–8]. For such applications, UV emission below 340 nm normally is not desirable, as it leads to concerns about deep UV light induced toxicity [8–10]. To date, the utilization of conventional UV light sources for these applications has been severely limited by their relatively large size, low efficiency, and lack of flexibility. Such critical issues can be potentially addressed by the emerging nanowire light emitting diodes (LEDs), which can exhibit flexible device size, ranging from a single nanowire to a nanowire array. Moreover, nanowires can act as direct waveguides and lead to high efficiency light emission without sophisticated packaging and extra reflectors and lenses. The currently reported nanowire UV LEDs generally involve the use of ZnO, or ZnO/GaN heterostructures [11–15]. Such devices, however, exhibit a very high operation voltage, an unacceptably large resistance (1000 Ω, or larger), and an uncontrolled emission wavelength, due to the unstable p-type ZnO, the lack of carrier confinement, and the interfacial defects between ZnO and GaN. In addition, there has been no report on the device quantum efficiency for such nanowire devices. An alternative approach for achieving highly efficient UV emission is to use ternary $Al_xGa_{1-x}N$ nanowire structures. With tunable Al compositions, the emission from $Al_xGa_{1-x}N$ ternary alloys can cover the entire UV A–C range. Moreover, the difficulty in p-doping of the $Al_xGa_{1-x}N$ can be effectively addressed by novel designs, such as tunnel junction, polarization

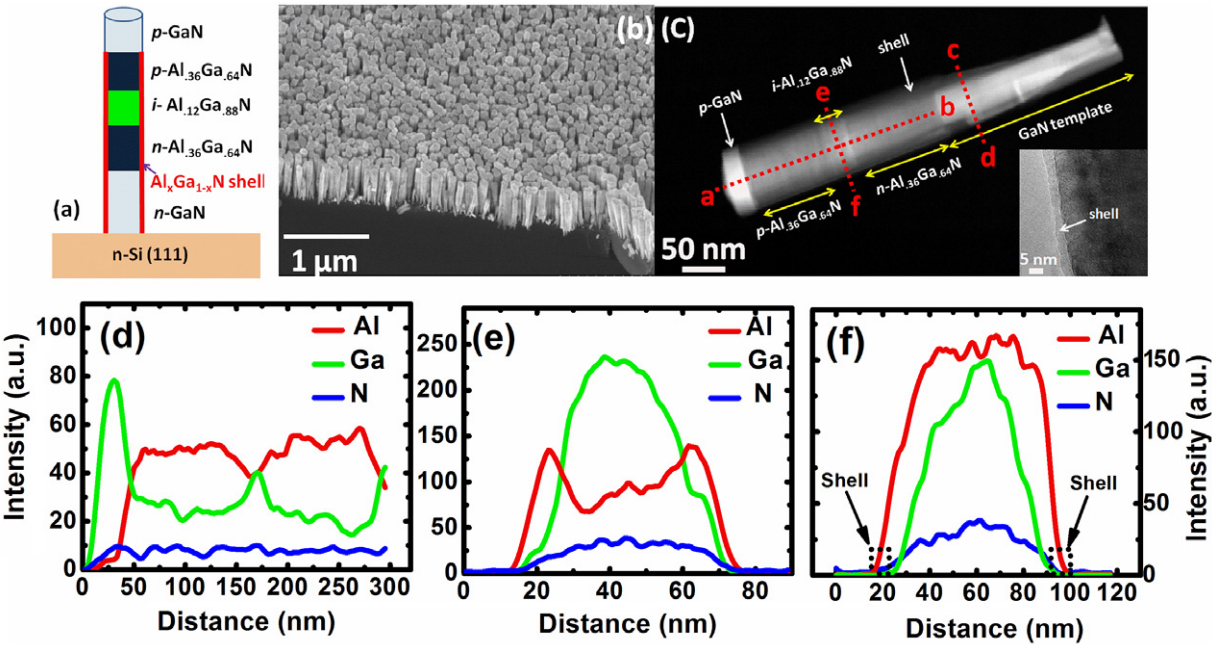

Figure 1. (a) Schematic diagram showing $Al_xGa_{1-x}N$ DH nanowire based LED structure. (b) Bird's eye view SEM image of nanowires on Si substrate. (c) HAADF-STEM image of single nanowire showing the structure of DH LEDs and Al-rich shell. Inset: HR-TEM image taken at the edge of the active region revealing the formation of shell around the sidewall of the nanowire. (d) Axial elemental profile measured along a–b line in (c) showing the DH structure. (e) and (f) Lateral elemental profile measured along the GaN template (c–d line in (c)) and active region (e–f line in (c)), respectively, showing core–shell structure.

enhanced Mg doping of AlGaN/GaN superlattices, and polarization induced holes in an Al compositionally graded junction [16–18]. The major difficulties for this material system arise from the growth of high quality $Al_xGa_{1-x}N$ nanowires with controlled directionality, uniformity, and tunability of the Al compositions. For example, during the catalyst-initiated growth of $Al_xGa_{1-x}N$ nanowires and related heterostructures, unintentional incorporation of metal catalyst into the materials could seriously degrade the optical and electrical properties of the devices [19]. Moreover, due to the absence of an effective carrier localization effect in such indium-free nitride materials, carriers can easily migrate to the surface of nanowires and thus nonradiative recombination on the sidewall of nanowires caused by surface states/defects severely limits the device efficiency [20].

In this regard, we have developed a special catalyst-free technique to grow highly uniform, vertically aligned $Al_xGa_{1-x}N$ nanowire based double heterojunction (DH) LEDs on top of GaN nanowire templates formed on a Si substrate. As a result of effective strain relaxation in the lateral direction, the crystal quality of nanowires can be greatly improved. Moreover, such $Al_xGa_{1-x}N$ nanowires exhibit unique core–shell structures, which can significantly suppress the nonradiative recombination associated with surface states/defects. In this communication, we successfully demonstrate highly efficient, spectrally pure $Al_xGa_{1-x}N$ nanowire array based DH LEDs operating at ~340 nm. Such nanowire devices exhibit superior electrical and optical performance, including an internal quantum efficiency (IQE) of ~59% at room temperature, a relatively small series resistance (~50–100 Ω), highly stable emission characteristics, and the absence of efficiency droop under pulsed biasing conditions.

2. Growth and structural characteristics

A schematic diagram of the $Al_xGa_{1-x}N$ nanowire is presented in figure 1(a). A Veeco Gen II molecular beam epitaxy (MBE) system equipped with a radio-frequency plasma-assisted nitrogen source was employed to grow the LED structure on n-Si(111). Before growth initiation, a thin (~0.6 nm) Ga seeding layer is firstly deposited. ~200 nm vertically aligned GaN nanowires with Si doping were spontaneously formed on Si(111) under nitrogen-rich conditions at 750–800 °C. This was followed by the deposition of ~100 nm $Al_{0.36}Ga_{0.64}N$:Si nanowire segments as an n-type cladding layer. After that, 40 nm $Al_{0.12}Ga_{0.88}N$ was grown as the active region and then a Mg doped $Al_{0.36}Ga_{0.64}N$ p-type cladding layer with a height of 100 nm was deposited. Finally, a 30 nm GaN layer doped with Mg was used as a contact layer. During growth, the nitrogen flow rate and plasma forward power were kept at 1 standard cubic centimeter per minute (SCCM) and 350 W, respectively. The growth rates of GaN and $Al_xGa_{1-x}N$ nanowires are ~3 nm min^{-1} and 2.5 nm min^{-1}, respectively. During the growth of the active region and cladding layers, the Al composition (x) was varied by controlling the Al/Ga flux ratios.

The sample morphology was examined by a high resolution scanning electron microscope (SEM). Shown in figure 1(b), the nanowires are vertically aligned on the substrate with excellent uniformity. The nanowire density is estimated to be 1×10^{10} cm^{-2}. Subsequently, A JEOL JEM-2100F scanning transmission electron microscope

(STEM) was used for annular dark field imaging and energy dispersive x-ray spectrometry (EDXS) analysis. For the STEM studies, the samples were prepared by transferring nanowires from the Si substrates to a Cu grid with a carbon supporting film. Figure 1(c) shows a high angle annular dark field (HAADF)-STEM image which is sensitive to the atomic number of the imaged material. The bright contrast regions at the bottom and top of the nanowire correspond to the GaN nanowire template and the p-type GaN contact regions, respectively. Additionally, the p- and n-type $Al_{0.36}Ga_{0.64}N$ cladding layers, and the intrinsic $Al_{0.12}Ga_{0.88}N$ active region can be identified based on the detailed studies described below. Shown in figure 1(d), the elemental profiles along the nanowire axial direction are derived from EDXS line scanning analysis along the growth direction (line a–b in figure 1(c)). As can be observed, in the top region of the nanowire, only Ga and N signals are presented, indicating the existence of a p-type GaN layer. Below the thin p-type GaN region, the rapid increase of the Al signal and the decrease of the Ga signal prove the formation of the $Al_xGa_{1-x}N$ cladding layer with a relatively high Al composition. Between the two cladding layers, an Al signal with a clear dip and a Ga signal with a peak can be observed, providing unambiguous evidence for the existence of a DH configuration along the nanowire axial direction.

It should be highlighted that, during the growth of the $Al_xGa_{1-x}N$ nanowire under nitrogen-rich conditions, a large amount of Al adatoms accumulate near the sidewall of the nanowire, due to a relatively short adatom diffusion length, resulting in the formation of an Al-rich $Al_xGa_{1-x}N$ shell on the nanowire lateral surfaces [21–25]. It has been confirmed that the formation of such an Al-rich shell structure can effectively suppress nonradiative recombination on the lateral surfaces of the active region and thus significantly improve the quantum efficiency. Shown in figure 1(c), a clear contrast between the bright inner core compared to the dark outer shell is observed, indicating the formation of a thin $Al_xGa_{1-x}N$ shell layer with higher Al composition in the radial direction around the sidewall of the nanowire. Due to the spontaneous formation of the AlGaN shell as well as the contribution to the shell from the subsequently grown AlGaN, the shell thickness is gradually varied from about 15 nm to a few nm with increasing height from the bottom GaN template to the top region of the nanowire. The presence of an Al-rich shell region may also be clearly observed from the high resolution TEM image taken at the edge of the $Al_{0.12}Ga_{0.88}N$ active region, shown in the inset of figure 1(c). Its thickness is determined to be ∼5 nm and is formed during the growth of the p-doped and undoped AlGaN layers. EDXS analyses were further performed to investigate the radial atomic distribution of the nanowire. The electron beam diameter is approximately 0.2 nm. The EDXS scanning lines and corresponding elemental profiles along the lateral direction of the bottom GaN template (line c–d in figure 1(c)) and active region (line e–f in figure 1(c)) are shown in figures 1(e) and (f), respectively. Shown in figure 1(e), across the GaN template region, the Al signals show a clear dip in the core region accompanied by two shoulders confirming the existence of an Al-rich shell. Around the $Al_{0.12}Ga_{0.88}N$ active region, shown in figure 1(f), the increase of the Al signal is also much faster than that of the Ga signal in the near-surface region of the nanowire, highlighted by the black boxes in figure 1(f). The less obvious shoulder feature measured in the active region (figure 1(f)), compared to that of the GaN nanowire template (figure 1(e)), is due to the relatively smaller shell thickness and lower Al compositional contrast between the core and shell of the active region.

3. Photoluminescence and internal quantum efficiency

Optical properties of the nanowire LED were investigated using temperature and power variable photoluminesecence (PL) spectroscopy. A 266 nm diode-pumped solid-state (DPSS) *Q*-switched laser was used as the excitation power source. The duration, maximum energy, and repetition rate of the laser pulse is ∼7 ns, 4 μJ, and 7.5 kHz, respectively. The signal was collected and analyzed by a high resolution spectrometer and detected by a photomultiplier tube. In order to perform power dependent PL, the excitation power was reduced using UV neutral density filters. A long pass filter (>270 nm) was placed in front of the spectrometer to eliminate emission from the excitation laser source. In temperature dependent PL measurements, the samples were placed into a helium closed-loop cryostat with temperature varying from 20 K to room temperature.

Figure 2(a) shows the normalized power dependent PL spectra measured at room temperature. At a very low excitation power, i.e., at 5 μW, PL emission from the $Al_{0.12}Ga_{0.88}N$ active region with a peak at 340 nm (E_1) dominates, which is attributed to effective carrier confinement in the active region. Moreover, two extra shoulders appear at ∼295 nm (E_2) and 310 nm (E_3), respectively. The E_2 peak corresponds to $Al_{0.36}Ga_{0.64}N$ cladding layers with higher Al compositions and the E_3 peak is most likely due to the defect associated radiative recombination in doped $Al_xGa_{1-x}N$. Such sub-band parasitic emission is often observed in $Al_xGa_{1-x}N$ multiple quantum well (MQW) based deep UV LEDs [26–28]. With increasing excitation power, the PL emission from the active region (E_1) begins to saturate, while the emission from the cladding layers (E_2 and E_3) is increased rapidly. This is mainly due to the fact that at high excitation power, photo-excited carriers with a higher thermal energy are more likely to escape from the active region and recombine in the cladding layers. Moreover, with increasing excitation power, the cladding layers themselves could also absorb more laser light and thus generate a stronger PL intensity. Finally, the emission at ∼364 nm from the GaN segment (E_4) can be observed at high excitation power.

We further performed temperature dependent PL studies from 20 to 300 K at an excitation power of 7 mW, shown in figure 2(b). It can be seen that at low temperature (20 K) the emission from the cladding layers (E_2 and E_3) is stronger than other peaks. This is mainly due to the fact that nonradiative recombination centers are largely inactive at low temperatures (∼10–20 K) and, consequently, the influence of nonradiative

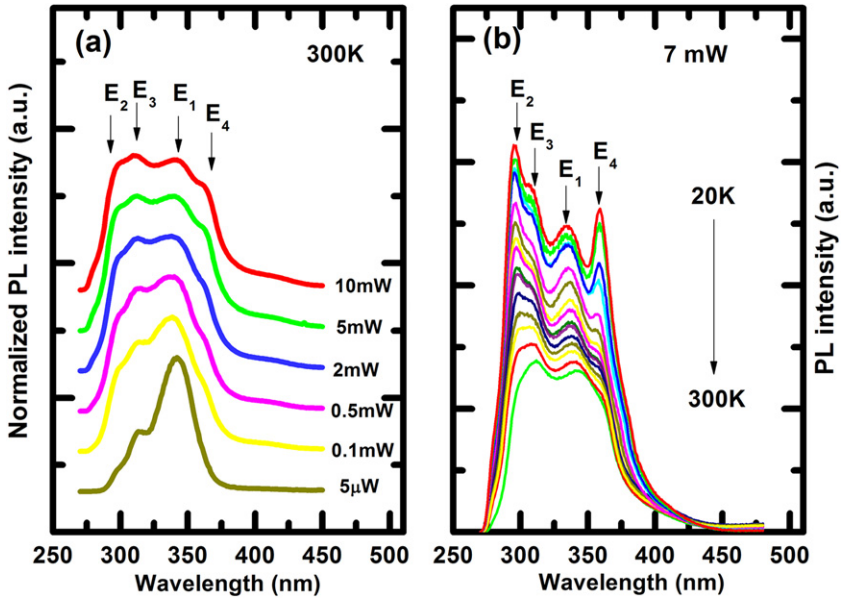

Figure 2. (a) Excitation power dependent PL spectra measured at room temperature. (b) Temperature dependent PL is investigated from 20 to 300 K with an interval of 20 K. Excitation power is 7 mW.

defects on the optical properties of the cladding layers can be negligible. Moreover, the strong absorption of laser light in the p-type cladding layer on the top of the nanowires and the relatively large material volume also contribute to the strong E_2 and E_3 peaks. For the same reasons, strong PL emission from doped GaN layers (E_4) is also present at low temperatures. However, with increasing temperature, the enhanced nonradiative recombination leads to a faster decrease of the E_2, E_3 and E_4 peaks due to higher Al compositions and/or doping induced defects in the cladding and GaN layers. In comparison, the reduction in the PL intensity of the E_1 peak from the intrinsic active region with higher crystal quality and better carrier confinement is much smaller with the increase of temperature from 20 and 300 K.

The IQE can be approximately estimated by comparing the integrated PL intensity measured at room temperature with respect to that measured at low temperature. Figure 3 shows the normalized integrated PL intensities of the whole spectra as a function of temperature in an Arrhenius plot. It is seen that at 7 mW excitation power the PL intensity at room temperature remains at about 46% of its intensity at 20 K, which is comparable to the previously reported IQE values for $Al_xGa_{1-x}N$ ternary nanowires measured under similar conditions [21]. The IQE of the active region at room temperature is further estimated based on the peak intensity at 340 nm at 7 mW excitation power. Shown in figure 3, the E_1 peak intensity at room temperature remains at about 59% of its intensity at 20 K. The resulting IQE of ∼59% is higher than that of the undoped $Al_xGa_{1-x}N$ nanowire measured under similar conditions. The enhancement in the IQE is mainly attributed to the effective carrier confinement of the active region in both the vertical and radial directions provided by the cladding layers and the unique shell structure, respectively.

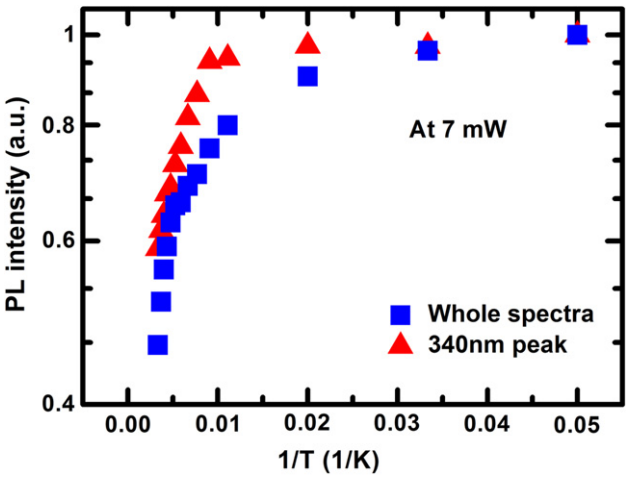

Figure 3. Arrhenius plots of PL integrated intensities measured from 20 to 300 K in semi-log scale. Room temperature IQEs for the whole spectra and active region are estimated to be 46% and 59%, respectively.

4. Device fabrication and characteristics

The fabrication of $Al_xGa_{1-x}N$ nanowire array based LEDs is carried out with a polyimide resist layer being used for the planarization and passivation of the nanowires [29]. An appropriate etch-back process using reactive ion etching was performed in order to allow for the exposure of the p-type layer of the nanowires. Before the deposition of the p-type metal contact, 49% HCl was used to remove any oxidized layer on the p-type GaN layer for 1 min. After that, a Ni (7.5 nm)/Au (7.5 nm) bi-layer was deposited at below 10^{-7} Torr by an electron beam evaporator and then annealed at 550 °C in N_2 for 1 min using a rapid thermal annealing (RTA) system. The n-type metal contact Ti (20 nm)/Au

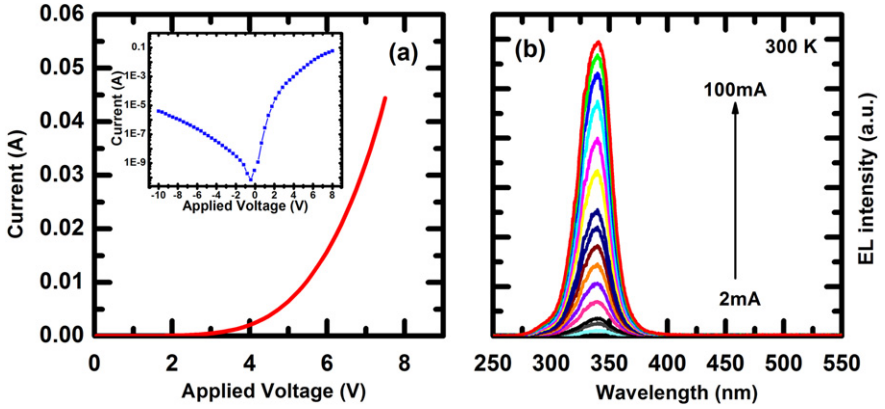

Figure 4. (a) Typical *I*–*V* curve for $Al_xGa_{1-x}N$ nanowire DH based LEDs with device size 300 μm × 300 μm. *I*–*V* characteristics of the device under forward and reverse bias in semi-log scale (inset). (b) Typical EL spectra measured at room temperature with different injection currents from 2 to 100 mA under CW biasing conditions.

(100 nm) was deposited at the backside of the n-type Si substrate and also annealed at 550 °C for 1 min via RTA. Finally, metallic contact grids with Ti (20 nm)/Au (150 nm) were made on the device surface to facilitate the carrier transport and injection process. Devices fabricated in different batches have been tested, and they exhibited similar *I*–*V* characteristics, demonstrating reliable device fabrication.

Figure 4(a) shows a typical *I*–*V* curve for nanowire based UV LEDs with an area of 300 μm × 300 μm. It exhibits excellent diode characteristics under forward bias, with 6.3 V at 20 mA injection current. The series resistance is estimated ∼50 Ω. Such results are significantly better than other nanowire based LEDs in the near UV region [11–15] and are also comparable with $Al_xGa_{1-x}N$ MQW based LEDs with the same peak emission wavelength [3, 30–34]. Achieving such good electrical properties for nanowire based LEDs can be partly attributed to the enhanced conductivity in III-nitride nanowires, due to the significant reduction in the formation energy for substitutional doping in the near-surface region of nanowires [35]. Also shown in the inset of figure 4(a), the leakage current under a reverse bias of −10 V is ∼4 × 10^{-6} A, which is slightly higher in comparison with the planar LEDs [36]. In the case of nanowire LEDs, insufficient insulation of polyimide resist between the nanowires could be a major source of leakage paths, thereby leading to a relatively high leakage current for the nanowire LEDs. Moreover, carriers recombining in the active region via surface states on the nanowire sidewall also contribute to the measured leakage current [37, 38]. Further investigation on the utilization of filling materials with high resistance and better sidewall passivation schemes is in progress in order to reduce the shorting paths along the nanowires.

Figure 4(b) shows typical EL spectra at room temperature with different injection currents from 2 to 100 mA under continuous wave (CW) biasing conditions. Devices tested from different areas of the wafer showed similar EL spectra, indicating good uniformity over the 2-in wafer. It can be observed that the device exhibits a strong and stable emission at 340 nm with the absence of any emission in the visible wavelength range, which was observed in $Al_xGa_{1-x}N$ MQW based UV LEDs, due to the deep level defects in $Al_xGa_{1-x}N$ [26, 39, 40]. Such a clean EL spectrum is important in the improvement of the signal–noise ratio and to eliminate the occurrence of fake results in discrimination of the NADH. Moreover, the emission peak position shows very small shifts (<2 nm) with increasing injection current, signifying the presence of a negligible polarization field due to the effective strain relaxation in the lateral direction of nanowires. The full-width-at-half-maximum (FWHM) for EL spectra is ∼30 nm and is nearly independent of injection currents.

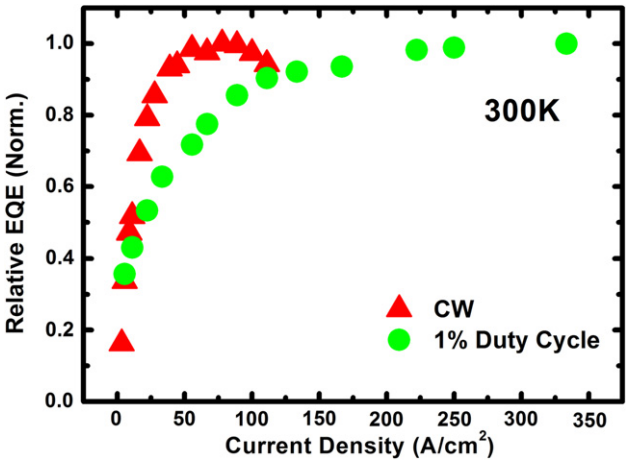

Figure 5. Relative EQEs of LEDs measured at room temperature using CW and pulsed injection current with 1% duty cycle showing the influence of the self-heating effect.

The relative external quantum efficiency (EQE) is measured under both CW and pulsed mode biasing conditions, as shown in figure 5. It is seen that efficiency droop is absent in such nanowire devices under pulsed biasing conditions (1% duty cycle) for injection currents up to ∼350 A cm^{-2} at room temperature. Compared to MQW based LEDs, $Al_xGa_{1-x}N$ nanowire structures can exhibit significantly reduced polarization fields and defect densities. Consequently, mechanisms that are largely responsible for efficiency droop in conventional LEDs, including

polarization field and defect-assisted Auger recombination, may become insignificant in nanowire LEDs [41]. However, the performance of $Al_xGa_{1-x}N$ LEDs suffers severely from a self-heating effect [42, 43], which leads to efficiency droop under CW driving current, as shown in figure 5. The reduced thermal conductivity of nanowires, compared to bulk materials also contributes to the heating effect. The heating effect can be potentially addressed by developing/utilizing suitable passivating materials with higher thermal conductivity in the fabrication of nanowire array based LEDs [44, 45].

5. Conclusion

In summary, we present a unique catalyst-free technique to grow uniform vertical arrays of $Al_xGa_{1-x}N$ nanowires with excellent crystal quality on a large area Si substrate. Such nanowires exhibit a thin Al-rich shell structure to effectively passivate the sidewalls of nanowires. Accordingly, the IQE of UV LEDs can be significantly enhanced. Finally, we successfully demonstrate $Al_xGa_{1-x}N$ nanowire based UV LEDs emitting at 340 nm with superior electrical and optical performance. Due to their strong, stable, and spectrally pure emission, fabrication of such $Al_xGa_{1-x}N$ nanowires in a flexible way to realize closed-loop controlled single nanowire devices will provide great potential in applications of nanobiosensors and implantable medical devices.

Acknowledgments

This work was supported by the Natural Sciences and Engineering Research Council (NSERC) of Canada. The device fabrication work was performed in the McGill University Nanotools Microfab facility.

References

[1] Davitt K, Song Y K, Patterson W III, Nurmikko A, Gherasimova M, Han J, Pan Y L and Chang R 2005 *Opt. Express* **13** 9548–55
[2] Xu H, Zhang J, Davitt K M, Song Y K and Nurmikko A V 2008 *J. Phys. D: Appl. Phys.* **41** 094013
[3] Peng H *et al* 2004 *Appl. Phys. Lett.* **85** 1436–8
[4] Mayevsky A and Rogatsky G G 2007 *Am. J. Physiol.* **292** C615–40
[5] Koo M, Park S Y and Lee K J 2012 *Nanobiosens. Dis. Diag.* **1** 5–15
[6] Miller G 2006 *Science* **314** 1674–6
[7] Venkataramani S, Davitt K M, Xu H, Zhang J, Song Y K, Connors B W and Nurmikko A V 2007 *J. Neurosci. Methods* **160** 5–9
[8] Rothman S M, Perry G, Yang X F, Hyrc K and Schmidt B F 2007 *Epilepsy Res.* **74** 201–9
[9] Chang Y, Xie Y and Weiss D S 2001 *J. Physiol.* **536** 471–8
[10] Leszkiewicz D N, Kandler K and Aizenman E 2000 *J. Physiol.* **524** 365–74
[11] Zhang X M, Lu M Y, Zhang Y, Chen L J and Wang Z L 2009 *Adv. Mater.* **21** 2767–70
[12] Bie Y Q *et al* 2010 *Adv. Mater.* **22** 4284–7
[13] Lupan O, Pauporté T and Viana B 2010 *Adv. Mater.* **22** 3298–302
[14] Chen M T, Lu M P, Wu Y J, Song J, Lee C Y, Lu M Y, Chang Y C, Chou L J, Wang Z L and Chen L J 2010 *Nano Lett.* **10** 4387–93
[15] Jha S K, Luan C, To C H, Kutsay O, KovaC J J, Zapien J A, Bello I and Lee S T 2012 *Appl. Phys. Lett.* **101** 211116
[16] Krishnamoorthy S, Akyol F, Park P S and Rajan S 2013 *Appl. Phys. Lett.* **102** 113503
[17] Yasan A, McClintock R, Darvish S R, Lin Z, Mi K, Kung P and Razeghi M 2002 *Appl. Phys. Lett.* **80** 2108–10
[18] Simon J, Protasenko V, Lian C, Xing H and Jena D 2010 *Science* **327** 60–4
[19] Chèze C *et al* 2010 *Nano Res.* **3** 528–36
[20] Chichibu S F *et al* 2006 *Nature Mater.* **5** 810–6
[21] Wang Q, Nguyen H P T, Cui K and Mi Z 2012 *Appl. Phys. Lett.* **101** 043115
[22] Allah R F, Ben T, Songmuang R and Gonzalez D 2012 *Appl. Phys. Express* **5** 045002
[23] Jindal V and Shahedipour Sandvik F 2009 *J. Appl. Phys.* **105** 084902
[24] Shitara T, Neave J H and Joyce B A 1993 *Appl. Phys. Lett.* **62** 1658–60
[25] Songmuang R, Ben T, Daudin B, González D and Monroy E 2010 *Nanotechnology* **21** 295605
[26] Zhang J, Wu S, Rai S, Mandavilli V, Adivarahan V, Chitnis A, Shatalov M and Khan M A 2003 *Appl. Phys. Lett.* **83** 3456–8
[27] Zhou L, Epler J E, Krames M R, Goetz W, Gherasimova M, Ren Z, Han J, Kneissl M and Johnson N M 2006 *Appl. Phys. Lett.* **89** 241113
[28] Zhang J C, Zhu Y H, Egawa T, Sumiya S, Miyoshi M and Tanaka M 2008 *Appl. Phys. Lett.* **93** 131117
[29] Nguyen H P T, Zhang S, Cui K, Han X, Fathololoumi S, Couillard M, Botton G A and Mi Z 2011 *Nano Lett.* **11** 1919–24
[30] Wang T, Lee K B, Bai J, Parbrook P J, Airey R J, Wang Q, Hill G, Ranalli F and Cullis A G 2006 *Appl. Phys. Lett.* **89** 081126
[31] Oder T N, Kim K H, Lin J Y and Jiang H X 2004 *Appl. Phys. Lett.* **84** 466–8
[32] Kim K H, Li J, Jin S X, Lin J Y and Jiang H X 2003 *Appl. Phys. Lett.* **83** 566–8
[33] Jeon S-R *et al* 2004 *Japan. J. Appl. Phys.* **43** L1409
[34] Smith G A, Dang T N, Nelson T R, Brown J L, Tsvetkov D, Usikov A and Dmitriev V 2004 *J. Appl. Phys.* **95** 8247–51
[35] Zhao S, Fathololoumi S, Bevan K H, Liu D P, Kibria M G, Li Q, Wang G T, Guo H and Mi Z 2012 *Nano Lett.* **12** 2877–82
[36] Wang T *et al* 2008 *J. Phys. D: Appl. Phys.* **41** 094003
[37] Bai J, Wang Q and Wang T 2012 *J. Appl. Phys.* **111** 113103
[38] Lee Y J, Lee C J, Chen C H, Lu T C and Kuo H C 2011 *IEEE J. Sel. Top. Quantum Electron.* **17** 985–9
[39] Chen K X, Xi Y A, Mont F W, Kim J K, Schubert E F, Liu W, Li X and Smart J A 2007 *J. Appl. Phys.* **101** 113102
[40] Park J S, Fothergill D W, Wellenius P, Bishop S M, Muth J F and Davis R F 2006 *Japan. J. Appl. Phys.* **45** 4083
[41] Nguyen H P T, Cui K, Zhang S, Djavid M, Korinek A, Botton G A and Mi Z 2012 *Nano Lett.* **12** 1317–23
[42] Reed M L, Wraback M, Lunev A, Bilenko Y, Hu X, Sattu A, Deng J, Shatalov M and Gaska R 2008 *Phys. Status Solidi* c **5** 2053–5
[43] Chitnis A *et al* 2002 *Appl. Phys. Lett.* **81** 3491–3
[44] Zhou Y, Wang L, Zhang H, Bai Y, Niu Y and Wang H 2012 *Appl. Phys. Lett.* **101** 012903
[45] Li T L and Hsu S L C 2010 *J. Phys. Chem.* B **114** 6825–9